ρ_S	= solid density	$[kg \cdot m^{-3}]$
σ_L	= liquid surface tension	$[N \cdot m^{-1}]$

〈Subscripts〉

est.	= estimated value
obs.	= observed value
0	= without solid particles

Literature Cited

1) Akita, K. and F. Yoshida: *Ind. Eng. Chem., Process Des. Develop.*, **12**, 76 (1973).
2) Deckwer, W.-D., Y. Louisi, A. Zaidi and M. Ralek: *Ind. Eng. Chem., Process Des. Develop.*, **19**, 699 (1980).
3) Himmelblau, D. M.: "Process Analysis by Statistical Methods," p. 178, John Wiley & Sons (1970).
4) Kara, S., B. G. Kellar and Y. T. Shah: *Ind. Eng. Chem., Process Des. Develop.*, **21**, 584 (1982).
5) Kato, Y., A. Nishiwaki, T. Kago, T. Fukuda and S. Tanaka: *Kagaku Kōgaku*, **36**, 1333 (1972).
6) Kato, Y., A. Nishiwaki, T. Fukuda and S. Tanaka: *J. Chem. Eng. Japan*, **5**, 112 (1972).
7) Kawagoe, M., T. Inoue, K. Nakano and T. Otake: *Kagaku Kōgaku*, **38**, 733 (1974).
8) Koide, K., T. Hirahara and H. Kubota: *Kagaku Kōgaku*, **30**, 712 (1966).
9) Koide, K., H. Sato and S. Iwamoto: *J. Chem. Eng. Japan*, **16**, 407 (1983).
10) Kojima, H. and K. Asano: *Kagaku Kogaku Ronbunshu*, **6**, 47 (1980).
11) Marrucci, G.: *Ind. Eng. Chem., Fundam.*, **4**, 224 (1965).
12) Maruyama, T., S. Yoshida and T. Mizushina: *J. Chem. Eng. Japan*, **14**, 352 (1981).
13) Ohki, Y. and H. Inoue: *Chem. Eng. Sci.*, **25**, 1 (1970).
14) Sakata, M. and T. Miyauchi: *Kagaku Kogaku Ronbunshu*, **6**, 428 (1980).
15) Shah, Y. T.: "Gas-Liquid-Solid Reactor Design," McGraw Hill, New York (1979).
16) Yamashita, F. and H. Inoue: *J. Chem. Eng. Japan*, **8**, 334 (1975).

(Presented in part at the 16th Autumn Meeting of the Society of Chemical Engineers, Japan, Toyota, October 6, 1982 and at the Third Pacific Chemical Engineering Congress, Seoul, Korea, May 11, 1983.)

FLOW CHARACTERISTICS IN A CHANNEL WITH SYMMETRIC WAVY WALL FOR STEADY FLOW

TATSUO NISHIMURA, YOSHIJI OHORI AND YUJI KAWAMURA

Department of Chemical Engineering, Hiroshima University, Higashi-Hiroshima 724

Key Words: Fluid Mechanics, Friction Factor, Wall Shear Stress, Flow Visualization, Electrochemical Method, Finite Element Method

Flow characteristics in a channel with a symmetric wavy wall were investigated by calculations and experiments. The channel used has a geometry similar to that of the Oxford membrane blood oxygenator. The flow regime covered ranged from laminar to turbulent flow.

The variation of pressure drop and wall shear stress with the Reynolds number was elucidated by the behavior of the circulated vortex formed at the diverging cross section of the channel.

Introduction

The channel or tube with wavy wall is one of several devices employed for enhancing the heat and mass transfer efficiency of processes having high Peclet numbers, such as compact heat exchangers with high heat flux and membrane blood oxygenators in extra-corporeal system, etc.

Chow *et al.*[2,3] solved analytically the flow in the channel and tube. Fedkiw *et al.*[5] obtained the solution for the tube in the creeping flow region by a collocation method. Deiber *et al.*[4] used a finite difference method for the same geometry beyond the Reynolds number at which inertial effects are important. They also measured the friction factor, and obtained good agreement between experiment and calculation. These results give the stream patterns and friction factors in the channel or tube. There has been, however, little work about the wall shear stress, which is an important factor for the prediction of the heat and mass transfer rates of systems with high Peclet numbers.

In this study we employed a channel with a symmetric sinusoidal wavy wall, which has a geometry

Received September 16, 1983. Correspondence concerning this article should be addressed to T. Nishimura. Y. Ohori is now with Mitsui Petrochemical Co., Ltd., Kugagun 740.

similar to that of the Oxford membrane oxygenator of Bellhouse *et al.*[1] The friction factor and wall shear stress in the fully developed flow region were measured and flow observations were performed in the Reynolds number range 100 to 10,000 based on the mean height and mean velocity of the channel. Furthermore, theoretical solutions were obtained by a finite element method in the laminar flow region and were compared with experiments.

1. Experimental Apparatus

A schematic representation of the flow system used in this study is shown in **Fig. 1**. A steady flow was supplied to the test section by a head tank. The flow rate was controlled by control valves and measured by an orifice flow meter. The test section consisted of a pair of sinusoidal wavy plates placed symmetrically about the flow axis, with a mean gap of 13 mm as shown in **Fig. 2** and the aspect ratio of the cross section W/H_{av} was 15.38. The entrance section with a length of 2000 mm was located at the upstream end of the test section. Each wavy plate had an amplitude-to-length ratio $2a/\lambda$ of 0.25 and ten crests separated by a distance of 28 mm.

2. Experimental Procedure

Measurements of axial pressure drop were made using taps connected to 0.8 mm holes which were drilled through a wavy plate as shown in Fig. 2. The fluids used were aqueous solution of 40% glycerol and city water. This measurement was performed in the Reynolds number range 40 to 10,000.

The wall shear stress along the wavy surface was measured by an electrochemical method developed by Hanratty[7] and Mizushina.[8] A diffusional current i_d is related to the wall shear stress τ_w*[1] from the Leveque theory:

$$\tau_w = 3.55 \times 10^{-15}\, \mu i_d^3/(C_b^3 d^5 \mathscr{D}^2) \qquad (1)$$

This equation holds for steady or quasi-steady boundary layer flows. The diffusional current was obtained by using 0.5 mm diameter platinum wires at nine chordwise locations along the surface of the eighth wave, as shown in Fig. 2. The electrolyte used had a composition of 0.01 N potassium ferri-ferro cyanide and 1.0 N sodium hydroxide. The shear stress measurement was performed in the Reynolds number range 350 to 10,000.

The flow observations were performed by the hydrogen bubbles method in the Reynolds number range 40 to 10,000. Nine strip electrodes were placed at the same positions on the surface as were used for the shear stress measurements. These electrodes were 0.05 mm thick by 30 mm long and were aligned with the width of a wavy plate. The flow near the wall was visualized by the bubbles generated at these electrodes, which determined the flow separation and reattachment points. In addition to the electrodes located on the wavy surface, another electrode was placed upstream of the measuring section to isolate the behavior of the mainstream from that near the wall.

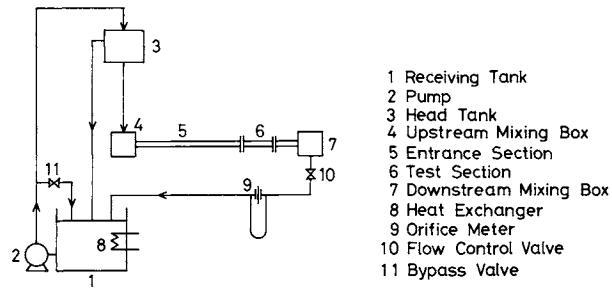

Fig. 1. Flow system.

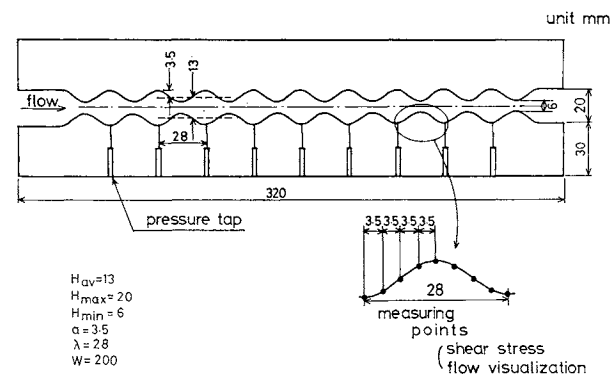

Fig. 2. Details of test section.

3. Theoretical Calculation

A theoretical investigation was carried out by a two-dimensional, finite-element method, as previously described by Nishimura *et al.*[9] This analysis postulates a laminar steady flow range only, because it is very difficult to treat turbulent flow with separation at the present time. The fluid motion was expressed in terms of the vorticity and the stream function. A successive approximation of Payatake *et al.*[10] was adopted in order to ensure the solution in the fully developed flow. Because of the symmetry of the flow, only the half of the channel was considered, and the analysed flow field was divided into 1120 elements with 627 nodal points. Computations were carried out in the Reynolds number range 1 to 700.*[2]

*[1] Since the wall shear stress is proportional to the electrode diameter raised to the -5 power as shown by Eq. (1), it is necessary to accurately determine the electrode diameter. This value tends to change in the electrode embedding process. In this study the diameters measured by a microscope after the electrode embedding process were employed.

*[2] As described in the section of results and discussion, the theoretical solutions agreed well with the experiments until about $Re = 350$, but disagreed at larger Reynolds numbers. The reason for this is that although the actual flow pattern becomes unsteady at Reynolds numbers above 350, the theory considers steady flow.

4. Results and Discussion

4.1 Flow pattern

The calculated stream lines are shown in **Fig. 3**. The stream lines at $Re=1$ are symmetrical about the maximum cross section of the channel. This indicates that inertial effects are not important. The stream lines become asymmetrical with increasing Reynolds number, and the circulated vortex is first formed upstream of the maximum cross section of the channel at $Re=15$. At larger Reynolds numbers, the vortex grows further, its center shifts downstream. Also, its circulation increases with Reynolds number.

Figure 4 shows the photographs of the flow pattern in the test section. The mainstream passes the central part of the channel and stable twin (symmetrical about the flow axis) circulated vortices are formed at the maximum cross section as shown in the photograph at $Re=95$. So convective mixing between the mainstream and the vortex hardly occurs, and the separation and reattachment points are fixed. This flow pattern is kept until about $Re=350$. As the Reynolds number increases further, the vortex changes from steady to unsteady motion, i.e., the vortex size varies with time. This behavior is not periodical but is an intermittent phenomenon. The photograph at $Re=670$ shows that the mainstream is violently-disturbed by the unsteady vortex motion. The flow pattern at larger Reynolds numbers shows similar behavior to that at $Re=670$, but the intensity and frequency of vortex motion is much reinforced.

Comparison of calculated and observed vortices at $Re=100$ is shown in **Fig. 5**. Both results are in good agreement on the vortex size. The above calculations and experiments indicate two flow regions. Laminar flow exists at Reynolds numbers less than about 350, and a subsequent increase of Reynolds number causes turbulent flow to develop.

The circulation zone between separation and reattachment points is shown in **Fig. 6** for the variation of Reynolds number. The dotted line is the calculated curve which is determined from the stream lines as shown in Fig. 3 and the solid line indicates the experimental curve which is determined from the local flow observations near the wall. For the laminar flow region, the circulation zone appears at $Re=15$ and the extent of this zone increases with Reynolds number. The measured values are consistent with the calculated values. For the turbulent flow region, the measured separation point gradually shifts upstream with increasing Reynolds number and tends to reach a limiting value ($x/\lambda=0.07$) at Reynolds numbers greater than 3000. The reattachment point is not fixed but is fluctuating, in contrast to the case of the separation point. The average reattachment point shifts upstream with increasing Reynolds number and approaches a limiting value ($x/\lambda=0.75$). The calculated reattachment point dis-

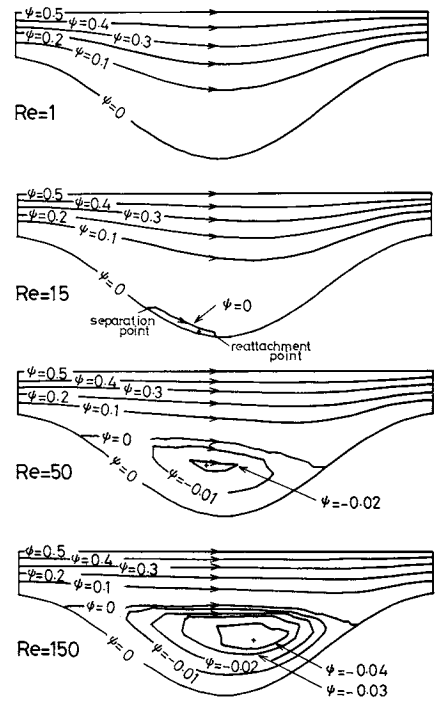

Fig. 3. Calculated stream lines at various Reynolds numbers.

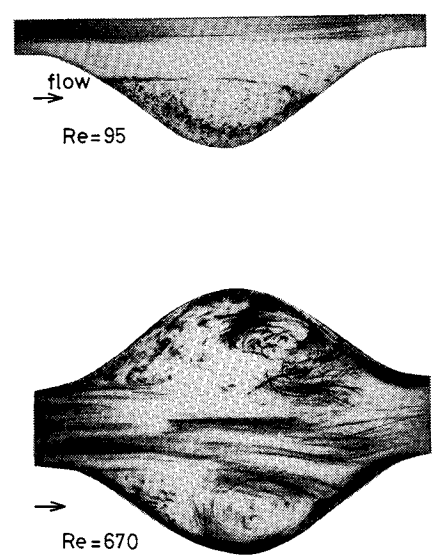

Fig. 4. Photographs of flow pattern at specified Reynolds numbers.

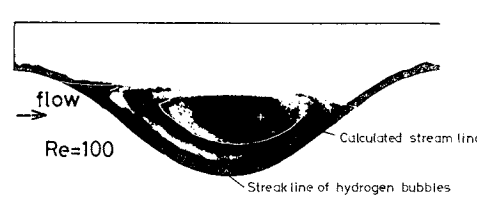

Fig. 5. Comparison of calculated and observed vortices at $Re=100$.

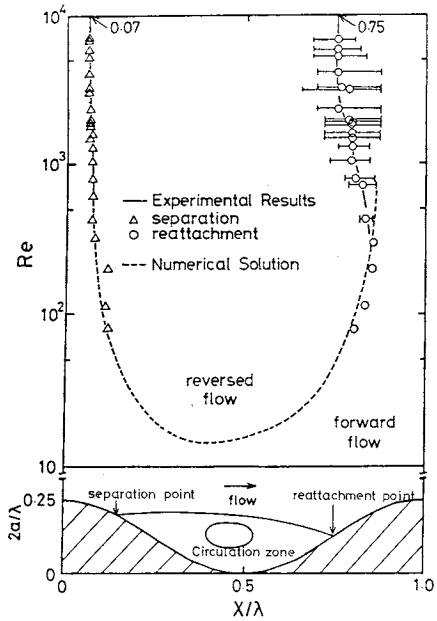

Fig. 6. Variation in separation and rettachment points with Reynolds number.

agrees with the measured value if the Reynolds number is greater than 350. The reason for this is that the calculation is treated as the steady state, though the actual flow pattern shows the unsteady vortex motion. Thus it is noted that the circulation zone expands with Reynolds number for the laminar flow but this zone contracts and approaches a limiting value for turbulent flow. Similar results have been observed for the case of abrupt expansion.[11]

4.2 Pressure drop

The relationship between friction factor and Reynolds number is shown in **Fig. 7**. For low Reynolds numbers (laminar flow region), the calculated friction factor*[3] represented by the dotted line decreases monotonically with the slope of -1 until $Re=15$. This Reynolds number corresponds to the appearance of the circulation zone. Furthermore, the slope gradually decreases with increasing Reynolds number. The measured values are in good agreement with the calculated values until about $Re=350$. In the turbulent flow region, the measured friction factor has a small peak and then becomes almost constant with increasing Reynolds number. This peak zone is related to the flow transition.

4.3 Wall shear stress

The calculated wall vorticity profiles are shown in **Fig. 8**. The vorticity at $Re=1$ has a positive value and its profile is a symmetrical concave shape about the maximum cross section. As the Reynolds number increases, the vorticity near the maximum cross section becomes negative, corresponding to the appearance of the circulation zone shown in Fig. 3, and

*[3] The calculation of friction factor is the same procedure as that of Kanaoka *et al.*[7]

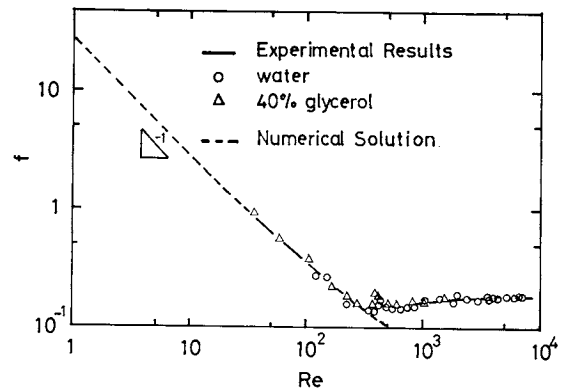

Fig. 7. Friction factor versus Reynolds number.

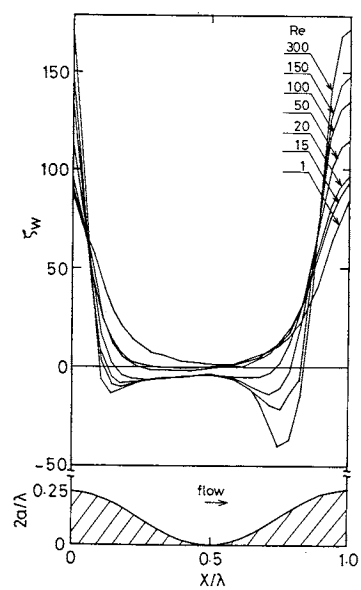

Fig. 8. Calculated wall vorticity profiles at various Reynolds numbers.

the minimum point of the vorticity appears slightly upstream from the reattachment point at Reynolds numbers greater than 100.

The measured wall shear stress profiles are shown in **Fig. 9**. Open symbols in this figure represent the forward flow and filled symbols are used for the reversed flow. This determination was made by flow observations in the manner described above. As shown in Fig. 9(a), the wall shear stress in the reversed flow zone (circulation zone) for low Reynolds numbers is extremely smaller than that in the forward flow zone and the maximum value is located at the minimum cross section. In Fig. 9(b), the wall shear stress in the reversed flow zone at high Reynolds numbers has a peak with increasing Reynolds number, and the maximum point of the shear stress slightly shifts downstream from the minimum cross section.

Comparison between calculated and measured vorticity profiles for $Re=350$ is illustrated in **Fig. 10**. Good agreement is obtained on the whole, thus validating the experimental technique.

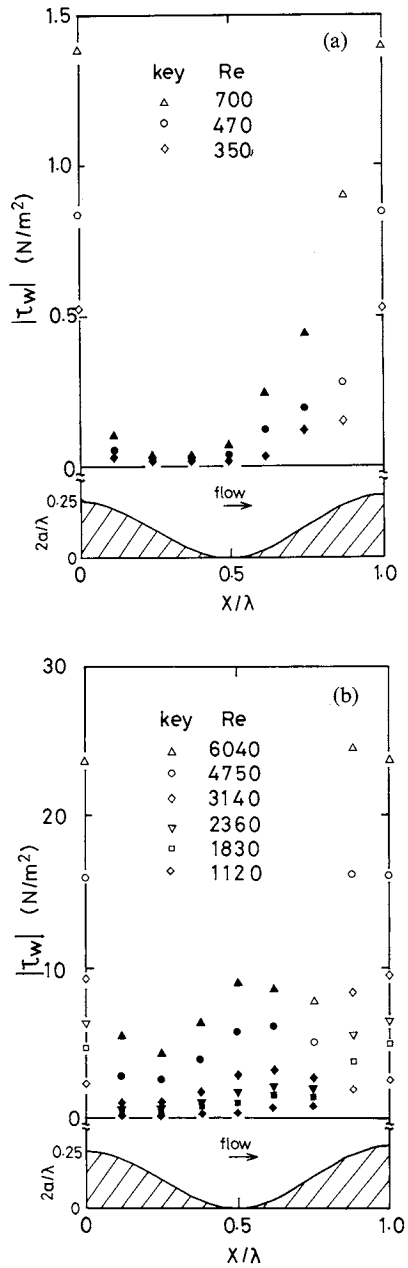

Fig. 9. Measured wall shear stress profiles at various Reynolds numbers.

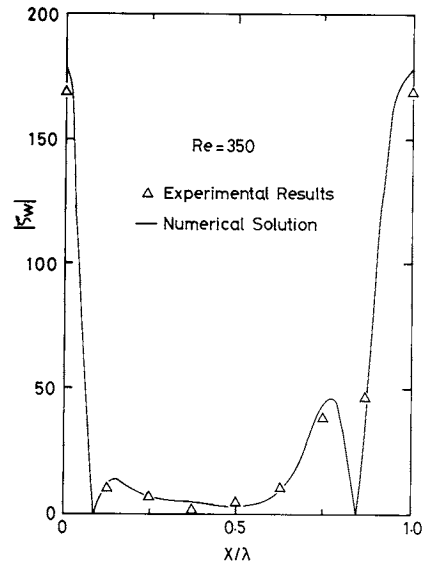

Fig. 10. Comparison of calculated and measured vorticity profiles at $Re=350$.

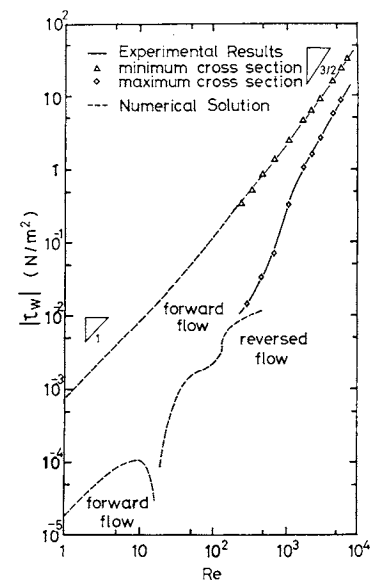

Fig. 11. Local shear stress versus Reynolds number.

The relationship between wall shear stress and Reynolds number is shown in **Fig. 11**, which includes the above calculated and experimental results. The wall shear stress at the minimum cross section increases monotonically with Reynolds number. The calculated values increase with the slope of 1 until $Re=15$ and after that the slope gradually increases with Reynolds number. The measured values lie on the extension of the calculated line. The wall shear stress increases further at larger Reynolds numbers and the slope becomes 3/2. At the maximum cross section, the variation of wall shear stress with Reynolds number is not monotonous. The calculated line becomes discontinuous at $Re=15$. This phenomenon shows that the flow at the maximum cross section changes from forward to reverse direction, i.e., the circulation zone appears. The plateau appears in the Reynolds number range 50 to 100. The measured wall shear stress tends to agree with the calculation and then increases with Reynolds number. A significant increment occurs in the Reynolds number range 350 to 1000, which corresponds to the peak zone of friction factor shown in Fig. 7, i.e., the flow transition from laminar to turbulent motion. Thus it is deduced that the unsteady vortex motion in the turbulent flow region remarkably affects the flow near the wall at the diverging cross section.

Conclusions

The flow characteristics in a wavy channel were

obtained by calculations and experiments.

1) For the wavy channel used in this study, laminar flow exists at Reynolds numbers less than 350, and a subsequent increase of Reynolds number causes turbulent flow to develop, owing to the onset of unsteady vortex motion.

2) The relationship between circulation zone and Reynolds number was obtained. In the laminar flow range, the circulation zone expands with Reynolds number, but in the turbulent range this zone contracts and approaches a limiting value.

3) The relationship between friction factor and Reynolds number was obtained. In the laminar flow range, the friction factor is inversely proportional to Reynolds number, and in the turbulent range it is independent of Reynolds number.

4) The wall shear stress profiles were presented. The unsteady vortex motion significantly promotes wall shear stress at the maximum cross section, but it scarcely affects that at the minimum cross section.

Acknowledgment

The authors acknowledge with thanks the assistance of Messrs. Toru Takumi and Katsumi Mizuno in computation and experiment. This work was supported by the Science Research Foundation of the Ministry of Education, Science and Culture, Japan (Grant No. 58470092).

Nomenclature

a	=	wave amplitude	[m]
d	=	electrode diameter	[m]
f	=	friction factor $(=(1/4)(H_{av}/\lambda)(2\Delta P/\rho u_{av}^2))$	[—]
H_{av}	=	average spacing between wavy walls $(=(H_{max}+H_{min})/2)$	[m]
H_{max}	=	maximum spacing between wavy walls	[m]
H_{min}	=	minimum spacing between wavy walls	[m]
i_d	=	diffusional current	[A]
ΔP	=	pressure drop over one wave length	[kg·m/s^2]
Q	=	volumetric flow rate	[m^3/s]
C_b	=	bulk concentration	[kg·mol/m^3]
Re	=	Reynolds number $(=u_{av}H_{av}/\nu)$	[—]
u_{av}	=	velocity based on H_{av} $(=Q/(H_{av}\cdot W))$	[m/s]
s	=	velocity gradient	[l/s]
W	=	width of wavy wall	[m]
x	=	axial length	[m]
u_{max}	=	velocity based on H_{max} $(=Q/(H_{max}\cdot W))$	[m/s]
ξ_w	=	dimensionless normalized wall vorticity $(=s/(u_{max}/H_{max}))$	[—]
$\mathscr{D}$	=	molecular diffusivity	[m^2/s]
λ	=	wave length	[m]
ν	=	kinematic viscosity	[m^2/s]
μ	=	viscosity	[N·s/m^2]
ρ	=	density	[kg/m^3]
τ_w	=	wall shear stress	[N/m^2]
ψ	=	dimensionless normalized stream function	[—]

Literature Cited

1) Bellhouse, B. J.,F. H. Bellhouse, C. M. Curl, T. I. MacMillan, A. J. Gunning, E. H. Spratt, S. B. MacMurrung and J. M. Nelems: *Trans. Am. Soc. Artif. Int. Organs.*, **19**, 72 (1973).
2) Chow, J. C. F. and K. Soda: *Phys. Fluids*, **15**, 1700 (1972).
3) Chow, J. C. F. and K. Soda: *Trans. ASME J. Applied Mech.*, **40**, 843 (1973).
4) Deiber, J. A. and W. R. Schowalter: *AIChE J.*, **25**, 638 (1979).
5) Fedkiw, D. and J. Newman: *AIChE J.*, **23**, 255 (1977).
6) Hanratty, T. J.: *Pys. Fluids Suppl.*, **10**, S126 (1967).
7) Kanaoka, C., H. Emi, K. Nakada and T. Aikura: *Kagaku Kōgaku*, **38**, 223 (1974).
8) Mizushina, T.: "Advances in Heat Transfer," Vol. 7, p. 87, Academic Press (1971).
9) Nishimura, T. and Y. Kawamura: *J. Chem. Eng. Japan*, **14**, 267 (1981).
10) Payatake, A. C., C. Tien and R. M. Turian: *AIChE J.*, **19**, 58 (1973).
11) Roschke, E. J. and L. H. Back: *J. Biomech.*, **9**, 481 (1976).

(A part of this paper was presented at the Third Pacific Chemical Engineering Congress, at Seoul, Korea, May 1983.)